ARTICLE

Non-volatile Memory Devices Based on Polystyrene Derivatives with Electron-Donating Oligofluorene Pendent Moieties

Cheng-Liang Liu,[†] Jung-Ching Hsu,[†] Wen-Chang Chen,[*,†,‡] Kenji Sugiyama,[§] and Akira Hirao[*,§]

Department of Chemical Engineering and Institute of Polymer Science and Engineering, National Taiwan University, Taipei, Taiwan 10617, and Department of Organic and Polymeric Materials, Tokyo Institute of Technology, H-127, 2-12-1 Ookayama, Meguro-ku, Tokyo 152-8552, Japan

ABSTRACT We report bistable non-volatile memory devices based on polystyrene derivatives containing pendent electron-donating mono-, di-, and tri(9,9-dihexylfluorene), which are denoted as poly(**St-Fl**), poly(**St-Fl$_2$**), and poly(**St-Fl$_3$**), respectively. The effects of the oligofluorene chain lengths and polymer surface structures on the memory characteristics were explored. Poly(**St-Fl**)-, poly(**St-Fl$_2$**)-, and poly(**St-Fl$_3$**)-based devices exhibited a flash memory characteristic with different turn-on threshold voltages of 2.8, 2.0, and 1.8 V, respectively, which was on the reverse trend with the highest occupied molecular orbital levels of −5.86, −5.80, and −5.77 eV. Moreover, the memory device showed a high ON/OFF current ratio of 2.5×10^4 and a long retention time of 10^4 s. The possible mechanism of the switching behavior was explained by the space-charge-limited-current theory and filamentary conduction. The larger aggregation domain size of the polymer thin film processed from the mixed solvent of chlorobenzene/*N*,*N*-dimethylformamide probably promoted the diffusion of the Al atoms into the polymer film and formed the conduction channel. Thus, it significantly reduced the turn-on threshold voltage on the studied polymer memory devices. The present study suggested that the polymer memory characteristics could be efficiently tuned through the pendent conjugated chain length and surface structures.

KEYWORDS: memory • pendent polymers • oligofluorene • conjugated length • turn-on threshold voltage

INTRODUCTION

Resistive-type memories store data based on electrical bistability (ON and OFF states) at different voltage bias or current. They can be memorized with digital data by storing and discharging electrical charges. Most memory devices are commonly fabricated by the metal oxide technology. However, several organic and polymeric memory materials composed of sandwiched layers exhibited memory switching characteristics recently, including small molecules (1−3), conjugated polymers (4−8), non-conjugated polymers (functional polyimide systems (9−13) or polymers with specific pendent chromophores 14−19), and polymer nanocomposites (metal nanoparticle (20−23) or fullerene (24−27) embedded). The polymer-based memory devices had the advantages of low cost, design flexibility, and good processability as compared to the non-organic devices. The reported polymer memory types included write-once-read-many times (WORM) memory (12, 16, 17), flash memory (13−15), and dynamic random access memory (DRAM) (5, 9).

* Corresponding authors. Tel: +886-2-23628398 (W.-C.C.), +81-3-5734-2131 (A.H.). Fax: +886-2-23623040 (W.-C.C.), +81-3-5734-2887 (A.H.). E-mail: chenwc@ntu.edu.tw (W.-C.C.), ahirao@polymer.titech.ac.jp (A.H.).
Received for review May 21, 2009 and accepted August 17, 2009
† Department of Chemical Engineering, National Taiwan University.
‡ Institute of Polymer Science and Engineering, National Taiwan University.
§ Tokyo Institute of Technology.
DOI: 10.1021/am900346j
© 2009 American Chemical Society

The memory devices with two different states of conductance were realized through several proposed mechanisms such as the charge-transfer effect (9, 13, 20, 22), trapping/detrapping of charges (4, 5, 25), and filamentary conduction (14, 15, 19). It was believed that the polymer structure and morphology significantly affected the origin of the switching mode (2, 17). One of the pioneer studies by Kang et al. suggested that the highest occupied molecular orbital (HOMO) level of organic donor−acceptor polymers was in charge of the turn-on threshold voltage but the charge-transfer complex stability was primarily controlled by the dipole moment (9, 16, 18). Yang's group demonstrated that a Au nanoparticle embedded into the organic matrix could serve as a charge-trapping acceptor, which revealed the electrical bistability (20−22). Ree and his co-workers proposed the new thermally stable polyimide to tune the memory switching behavior with a high ON/OFF current ratio by controlling the compliance current (10, 11) or film thickness (8, 12). Polymers with the pendent electron-donating moiety, such as poly(*N*-vinylcarbazole) (PVK), exhibited programmable non-volatile memory application, and the mechanism was explained on the basis of the filament theory (14, 15). However, a systematic study on establishing the relationships between the chemical structure, polymer morphology, and memory characteristics has not been fully explored yet.

Polymers containing conjugated oligomers with precisely defined chain lengths represent a model system for investigating the structure−memory characteristic relationship. In this paper, memory devices based on polystyrene (PS)

Published on Web 09/01/2009

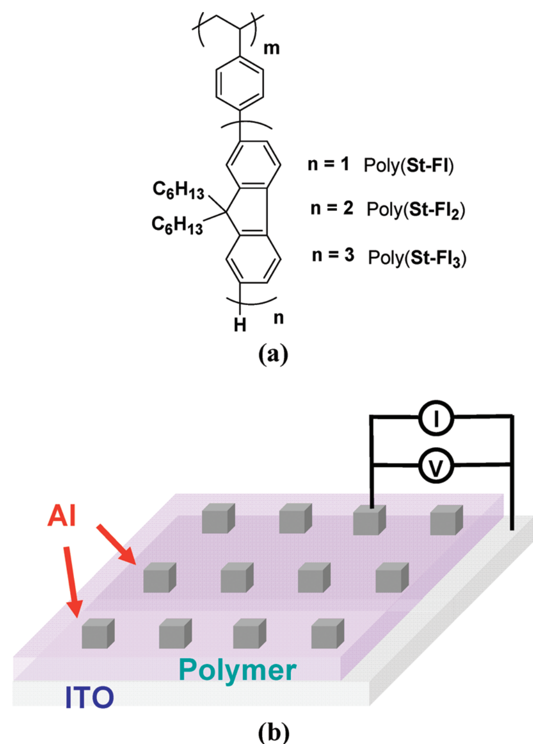

FIGURE 1. (a) Chemical structures of poly(St-Fl), poly(St-Fl_2), and poly(St-Fl_3). (b) Geometries of the ITO/polymer/Al memory device.

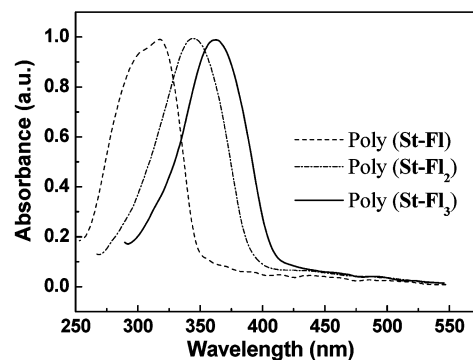

FIGURE 2. Absorption spectra of poly(St-Fl), poly(St-Fl_2), and poly(St-Fl_3) thin films prepared from CB after annealing.

derivatives para-substituted with mono-, di-, and tri(9,9-dihexylfluorene) units were fabricated and characterized and were denoted as (poly(**St-Fl**), poly(**St-Fl_2**), and poly(**St-Fl_3**), respectively. The chemical structures of the studied polymers are shown in Figure 1a. These polymers are soluble in common solvents, and thus uniform thin films could be obtained by spin coating. The different pendent oligofluorenes of the polymers were used to probe the hole injection/transporting barrier from the anode and turn-on threshold voltages of the memory devices. The switching model was analyzed by the space-charge-limited-current (SCLC) theory and metallic filament mechanism. The different polymer morphology was manipulated by a mixture of good (chlorobenzene, CB)/poor (*N*,*N*-dimethylformamide, DMF) solvents and correlated to the polymer memory characteristics. Our experimental results showed that the device performance was controlled by both the fluorene chain length and polymer morphology.

EXPERIMENTAL SECTION

Synthesis and Characterizations. The PS derivatives para-substituted with π-conjugated oligofluorene pendent moieties, poly(**St-Fl**), poly(**St-Fl_2**), and poly(**St-Fl_3**), were synthesized via anionic polymerization, as reported by us (28). A UV−vis optical absorption spectrum was obtained using a Hitachi U-4100 UV−vis spectrometer. The cyclic voltammograms (CVs) were recorded on a CHI 611B electrochemical analyzer using an indium−tin oxide (ITO) plate as the working electrode, Pt wire as the counter electrode, and Ag/AgCl as the reference electrode. A 0.1 M solution of tetrabutylammonium perchlorate (TBAP) in anhydrous acetonitrile was employed as the supporting electrolyte. The energy level of the HOMO was determined from the onset oxidation (E_{onset}^{ox}) and estimated on the basis of the reference energy level of ferrocence (4.8 V below the vacuum level) according to the following relation: HOMO $= -e(E_{onset}^{ox} - E_{ferrocene}^{1/2} + 4.8)$ (eV). The lowest unoccupied molecular orbital (LUMO) level was calculated from HOMO and the value of the optical band gap according to the relation LUMO $=$ HOMO $+ E_g^{opt}$ (eV) (13). The thickness of the polymer film was measured with a Microfigure Measuring Instrument (Surforder ET-3000, Kosaka Laboratory Ltd.). Atomic force microscopy (AFM) micrographs of the polymer film surface were obtained with a Nanoscope 3D Controller atomic force microscope (Digital Instruments) operated in the tapping mode at room temperature.

Fabrication and Measurement of the Memory Device. The non-volatile memory device, ITO/polymer/Al, was fabricated on precleaned glass substrates, as illustrated in Figure 1b. A total of 10 mg/mL of a well-dissolved polymer solution was spin-coated at 1000 rpm for 60 s onto the substrate. The monolayer polymer thin film was then annealed at 120 °C for 3 h under vacuum. The thickness of the thin film was determined to be about 20 nm. Finally, the 50-nm-thick Al top electrode was thermally evaporated through the shadow mask at a pressure of less than 10^{-7} Torr with a uniform rate of deposition of 3 Å/s. The electrical characterization of the memory device was performed by a Keithley 4200 semiconductor parameter analyzer in an ambient atmosphere without any encapsulation. The $I-V$ curves of the studied devices were measured in at least three runs during each stage to obtain the average value of the turn-on voltage.

RESULTS AND DISCUSSION

The studied polymers, poly(**St-Fl**), poly(**St-Fl_2**), and poly(**St-Fl_3**), for the memory device applications had similar molecular weights (M_n) of 11 500, 10 200, and 12 000 with very narrow distributions (PDI < 1.08), respectively. These polymers were soluble in common organic solvents such as tetrahydrofuran, chloroform, and CB but insoluble in the polar solvents DMF and dimethyl sulfoxide. Thus, CB and DMF served as good and poor solvents for tuning of the polymer morphology, respectively. The high-boiling-point CB and DMF solvents had slow evaporation speeds and might lead to the polymer chain packing more regularly at the annealing temperature of 120 °C, which was higher than the glass transition temperature of the polymers (T_g in the range of 75−78 °C).

The optical absorption spectra of the polymer thin films prepared from CB after annealing are shown in Figure 2. The absorption maxima of poly(**St-Fl**), poly(**St-Fl_2**), and poly(**St-Fl_3**) are observed at 318, 345, and 362 nm, respectively, which are attributed to the $\pi-\pi^*$ transition of the fluorene

ARTICLE

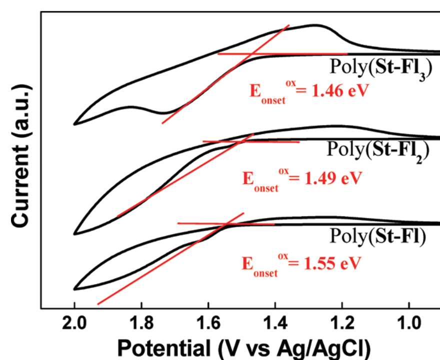

FIGURE 3. Cyclic voltammograms of poly(St-Fl), poly(St-Fl$_2$), and poly(St-Fl$_3$) in a 0.1 M TBAP/acetonitrile solution at a sweep rate of 100 mV/s.

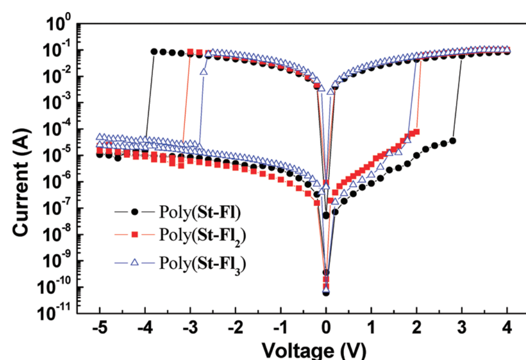

FIGURE 4. Typical $I-V$ curves of poly(St-Fl), poly(St-Fl$_2$), and poly(St-Fl$_3$) thin film (prepared from a CB solution) memory devices.

moiety (28). The red-shifted spectrum with increasing pendent fluorene chain length is attributed to the enhanced π-electron delocalization. The optical band gaps of poly(**St-Fl**), poly(**St-Fl$_2$**), and poly(**St-Fl$_3$**) estimated from the onset optical absorbance are 3.57, 3.20, and 3.05 eV, respectively. Figure 3 shows the CVs of the studied polymer films in a 0.1 M TBAP/acetonitrile solution at a sweep rate of 100 mV/s. The energy level of the HOMO was determined from the onset oxidation ($E_{\text{onset}}^{\text{ox}}$), assuming that the absolute energy of the level of Fc/Fc$^+$ was 4.8 eV below a vacuum. The HOMO energy levels of poly(**St-Fl**), poly(**St-Fl$_2$**), and poly(**St-Fl$_3$**) are estimated to be −5.86, −5.80, and −5.77 eV, respectively. This suggests that the HOMO level is enhanced with an increase in the pendent fluorene chain length and thus leads to better hole transport ability, similar to that reported in the literature (29). On the other hand, the LUMO energy levels of poly(**St-Fl**), poly(**St-Fl$_2$**), and poly(**St-Fl$_3$**) are −2.29, −2.60, and −2.72 eV, respectively, which are estimated from the difference between the HOMO level and optical band gap.

For the memory device, the polymers were dissolved in CB and spin-coated as thin films on the ITO glass. The polymer thickness was controlled at about 20 nm with reproducible switching. All of the electrical properties of the devices were measured at room temperature under an ambient atmosphere. Figure 4 shows the typical current−voltage ($I-V$) characteristics of the ITO/polymer/Al device, which are exhibited on a semilogarithmic scale. For comparison, a PS homopolymer shows a low current (<10^{-8} A) even with an increase in the applied voltage. This suggests that the PS-based device acts as an insulator without any memory effect (19, 27). By introduction of the pendent fluorene moieties, poly(**St-Fl**), poly(**St-Fl$_2$**), and poly(**St-Fl$_3$**) exhibit an interesting non-volatile memory and only change in the applied writing voltage. By taking the case of poly(**St-Fl**) as a example, the device is scanned through four voltage sequences: 0 to 4.0 V (first stage; write), 0 to 4.0 V (second stage; read), 0 to −5.0 V (third stage; erase), and 0 to −5.0 V (fourth stage; read) in steps of 0.2 or 0.1 V. The pristine device exhibits a low conductivity of 10^{-6} A at a low voltage of 1.0 V. As the positive voltage sweeps from 0 to 4.0 V (first stage), the current increases as the applied bias is enhanced. The device makes a sharp transition from the OFF state (low conductivity) to the ON state (high conductivity) roughly at the turn-on threshold voltage of 2.8 V. This electronic transition is viewed as the writing operation. The device remains in the ON state during the voltage sweep of the second stage and does not degrade to the initial state even after the power is turned off for at least 30 min. The electrical bistable poly(**St-Fl**) shows a maximum ON/OFF current ratio of 2.5×10^4 at 1.0 V. As the negative bias sweeps continuously from 0 to −5.0 V (third stage), the device switches back to the initial state with an abrupt current decrease of −4.0 V, indicating the erasing operation for the memory device. When the negative bias is subsequently applied (fourth stage), the device remains at a low conductivity. The bias can be further controlled by the same four stages, and the device exhibits reversible switching behavior between the ON and OFF transition. This typical bipolar nature can only be written on a positive bias and erased on a negative bias as verified several times. Therefore, poly(**St-Fl**), poly(**St-Fl$_2$**), and poly(**St-Fl$_3$**) could be flash-type memory devices with different turn-on threshold voltages of 2.8, 2.0, and 1.8 V, respectively. The above variation on the turn-on voltage may be explained as below. In the ITO/polymer/Al device, the energy barrier for the hole injection from the electrode to the active polymer layer (difference between the work function of ITO and the HOMO energy of the polymer) is estimated to be 0.97−1.06 eV. However, the energy barrier for the electron injection from the electrode to the active polymer layer (difference between the work function of Al and the LUMO energy of the polymer) is around 1.48−1.91 eV. Therefore, the charge conduction process of the memory device is mainly dominated by the hole injection. The lowest turn-on voltage of the poly(**St-Fl$_3$**) memory device is mainly attributed to the smallest hole injection barrier of 0.97 eV.

The double-logarithmic $I-V$ characteristics shown in Figure 5 are used to examine the electrical switching behavior. In the OFF state, the slope changes with increasing voltage bias as below: 1.0 (<0.6 V) and 2.0 (>0.6 V), indicating a transition from the ohmic to SCLC transport (23, 30, 31). At low voltages (<0.6 V), the hole begins to inject into the polymer thin film from the ITO and the current increases linearly with the voltage bias (ohmic conduction). The space charge accumulates with increasing voltage (>0.6 V) and is controlled through thermally active hopping conductions (7, 30, 31). After exceeding the turn-on threshold voltages,

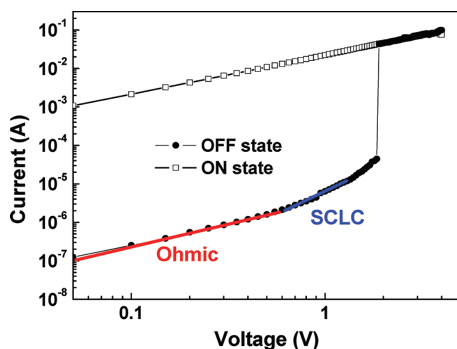

FIGURE 5. Log−log $I-V$ plot of the ON and OFF states based on the ITO/poly(St-Fl$_2$)/Al memory device.

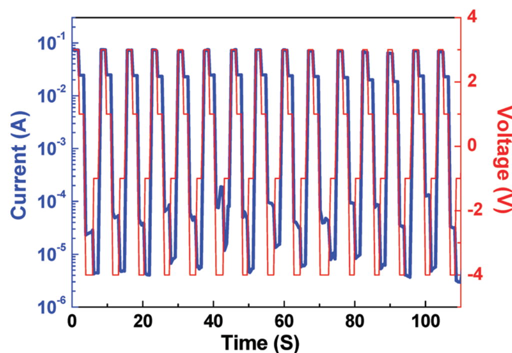

FIGURE 6. Current switching of the ITO/poly(St-Fl)/Al memory device during WRER cycles with the corresponding applied voltages.

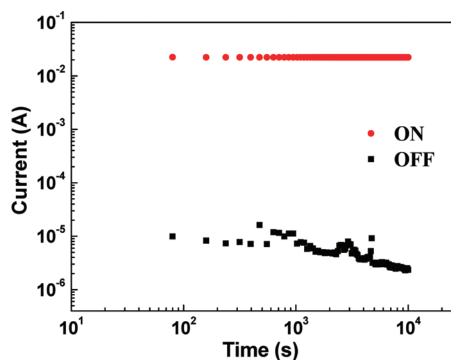

FIGURE 7. Retention times of the ON and OFF states of the ITO/poly(St-Fl)/Al memory device.

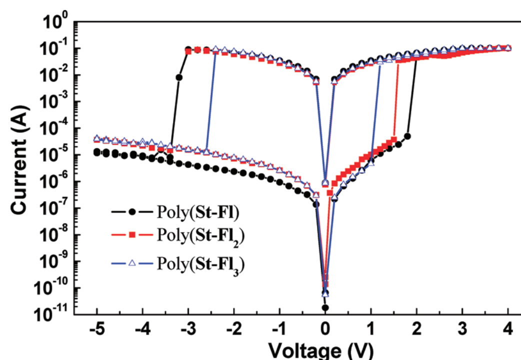

FIGURE 8. Typical $I-V$ curves of poly(St-Fl), poly(St-Fl$_2$), and poly(St-Fl$_3$) thin film (prepared from the CB/DMF mixed solvent) memory devices.

the current increases sharply around 4 orders of magnitude to a high-conductivity state, which indicates the formation of the metallic filament (14, 15, 32). The Al atoms with sufficient energy migrate inside the polymer layer, and the current flows between the upper Al and bottom ITO electrodes during the writing process. The linear $I-V$ relationship during the ON state is regarded as the formation of conductive filaments in the device. However, the ON current is insensitive to the three device areas (0.4 × 0.4, 0.5 × 0.5, and 0.6 × 0.6 mm^2), and thus the controlled formation and rupture of the filament conduction is probably responsible for the above memory effect (8, 11). As a result, both the SCLC model and filament conduction contribute to the switching behavior of the studied polymer memory devices. The ON/OFF switching of PVK (14, 15) and conjugated polymer (7, 8) memory devices was also found to be governed by the SCLC conduction and heterogeneous filament mechanism.

Programmable cyclic duration was performed by repeating the write-read-erase-reread (WRER) cycles. Figure 6 shows the voltage stressed on the device and the associate current response with the applied voltage. The voltages of write, read, erase, and reread for the poly(**St-Fl**)-based memory device are 3.0, 1.0, −4.0, and 1.0 V, respectively. The currents are recorded on the turn-ON, read-ON, turn-OFF, and read-OFF states. The duration of each WRER cycle remains constant at around 6 s with reproducible switching. The set of cyclic tests is continuously repeated, and the rewriting ability with the high ON/OFF current ratio confirms that the poly(**St-Fl**)-based device exhibits the non-volatile flash-type memory characteristic. Poly(**St-Fl$_2$**) and poly(**St-Fl$_3$**) also exhibit cyclic operations similar to that of poly(**St-Fl**). The difference in the oxidation stability causes the poly(**St-Fl$_3$**)-based device to only operate at 3−5 cycles. The retention time test on the memory device of poly(**St-Fl**) for the ON and OFF states is shown in Figure 7. Initially, the memory device starts to turn-ON or -OFF to a high or low conductivity state. The readout voltages of the ON and OFF states are 1.0 and −1.0 V, respectively. The current in both states does not change without any obvious degradation and is stable for at least 10^4 s. Similarly, the memory devices of poly(**St-Fl$_2$**) and poly(**St-Fl$_3$**) also maintain a good stability.

The performance of the memory device could be further improved by manipulating the polymer morphology through variation i the solvent polarity. Manipulation of the polymer morphology through the mixed solvent method has been widely reported in the literature (33−35). In this study, the synthesized polymers were well-dissolved in a pure good solvent (CB) and dropped into a poor solvent (DMF) with stirring. The optimizing CB/DMF ratio was about 9:1 (v/v) for the purpose of achieving a homogeneous polymer solution. All of the procedures and conditions of device fabrication were the same. Figure 8 shows the $I-V$ characteristics of the polymer memory device prepared from the CB/DMF (9:1, v/v) solution. The current increased around 4−5 orders of magnitude from the initial OFF state to the high ON state, followed by the erasing process in the next voltage sweep. The device still exhibited a flash-type switching memory

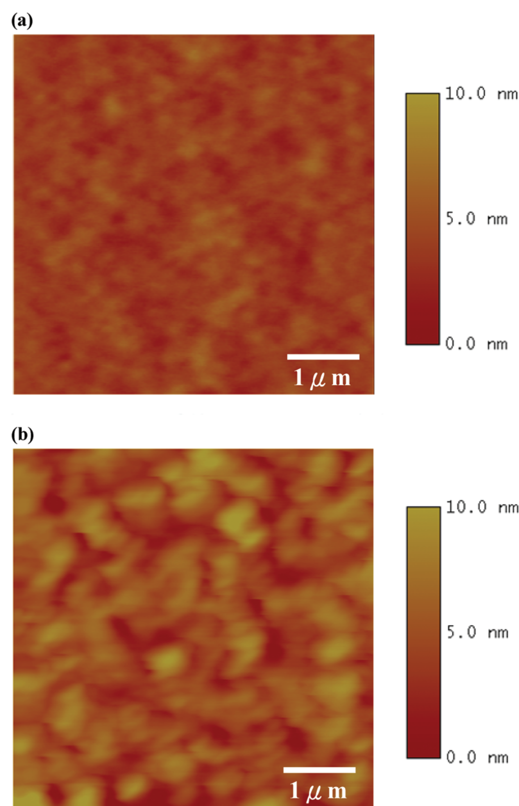

FIGURE 9. AFM height images (5 × 5 μm^2) of a poly(St-Fl_3) thin film prepared from (a) CB and (b) CB/DMF (9:1, v/v) for the memory device.

behavior. However, it was found that the addition of a poor solvent into the pristine polymer solution allowed tuning of the turn-on threshold voltage. The switching voltages of poly(**St-Fl**), poly(**St-Fl_2**), and poly(**St-Fl_3**) films were prepared from the CB/DMF mixed solvent changes from 2.8 to 1.8 V, from 2.0 to 1.9 V, ans from 1.5 to 1.0 V, respectively. The above result suggests that the switching threshold voltage is efficiently tuned by a change of the solvent power. Figure 9 shows the AFM images of the polymer thin films from the mixed solvent. Compared to the poly(**St-Fl_3**) thin film prepared from the CB solution (Figure 9a), a larger aggregation domain size from the CB/ DMF (9: 1, v/v) solution is observed in Figure 9b. The root-mean-square roughness estimated from Figure 9b is about 1.450 nm, which is larger than 0.232 nm from Figure 9a. The Al metal atoms diffused inside the polymer layer probably increase with the larger poly(**St-Fl_3**) aggregated domain and form the continuous electrical conduction channel (2, 17), which indeed enhances the switching conduction. The above result suggests the importance of polymer morphology in realizing the memory effect in addition to the conjugated chain-length effect.

CONCLUSIONS

In this study, we demonstrated the programmable switching non-volatile memory device fabricated from PS derivatives containing pendent oligofluorene moieties. Longer pendant chain lengths enhanced the HOMO level and thus reduced the turn-on threshold voltage. Moreover, the memory device showed a high ON/OFF current ratio of 2.5×10^4 and a long retention time of 10^4 s. The possible mechanism of the switching behavior was explained by the SCLC theory with filamentary conduction. The feasible results of the WRER cycle were also reproducibly observed on the studied memory device. The turn-on voltage of the studied memory devices could be further reduced by an increase in the aggregation domain size based on the mixed solvent approach. The present study suggested that the polymer memory characteristics could be efficiently tuned through the pendant conjugated chain length and surface structures.

Acknowledgment. Financial support of this work from the National Science Council, the Ministry of Economic Affairs, and the Excellence Research Program of National Taiwan University is highly appreciated.

Supporting Information Available: AFM images of poly(**St-Fl**) and poly(**St-Fl_2**) thin films prepared from CB and CB/DMF (9:1, v/v) for the memory device. This material is available free of charge via the Internet at http://pubs.acs.org.

REFERENCES AND NOTES

(1) Chen, J.; Ma, D. *Appl. Phys. Lett.* **2005**, *87*, 023505–023507.
(2) Lin, J.; Ma, D. *J. Appl. Phys.* **2008**, *103*, 024507–024510.
(3) Tu, C. H.; Lai, Y. S.; Kwong, D. L. *IEEE Electron Device Lett.* **2006**, *27*, 354–356.
(4) Ouisse, T.; Stephan, O. *Org. Electron.* **2004**, *5*, 251–256.
(5) Ling, Q. D.; Song, Y.; Lim, S. L.; Teo, E. Y. H.; Tan, Y. P.; Zhu, C.; Kang, E. T.; Neoh, K. G. *Angew. Chem., Int. Ed.* **2006**, *45*, 2947–2951.
(6) Baek, S.; Lee, D.; Kim, J.; Hong, S. H.; Kim, O.; Ree, M. *Adv. Funct. Mater.* **2007**, *17*, 2637–2644.
(7) Kim, T. W.; Oh, S. H.; Choi, H.; Wang, G.; Hwang, H.; Kim, D. Y.; Lee, T. *Appl. Phys. Lett.* **2008**, *92*, 253308–253310.
(8) Lee, T. J.; Park, S.; Hahm, S. G.; Kim, D. M.; Kim, K.; Kim, J.; Kwon, W.; Kim, Y.; Chang, T.; Ree, M. *J. Phys. Chem. C* **2009**, *113*, 3855–3861.
(9) Ling, Q. D.; Chang, F. C.; Sang, Y.; Zhu, C. X.; Liaw, D. J.; Chan, D. S. H.; Kang, E. T.; Neoh, K. G. *J. Am. Chem. Soc.* **2006**, *128*, 8732–8733.
(10) Hahm, S. G.; Choi, S.; Hong, S. H.; Lee, T. J.; Park, S.; Kim, D. M.; Kwon, W. S.; Kim, K.; Kim, O.; Ree, M. *Adv. Funct. Mater.* **2008**, *18*, 3276–3282.
(11) Hahm, S. G.; Choi, S.; Hong, S. H.; Lee, T. J.; Park, S.; Kim, D. M.; Kim, J. C.; Kwon, W. S.; Kim, K.; Kim, M. J.; Kim, O.; Ree, M. *J. Mater. Chem.* **2009**, *19*, 2207–2214.
(12) Lee, T. J.; Chang, C. W.; Hahm, S. G.; Kim, K.; Park, S.; Kim, D. M.; Kim, J.; Kwon, W. S.; Liou, G. S.; Ree, M. *Nanotechnology* **2009**, *20*, 135204–135210.
(13) You, N. H.; Chueh, C. C.; Liu, C. L.; Ueda, M.; Chen, W. C. *Macromolecules* **2009**, *42*, 4456–4463.
(14) Lai, Y. S.; Tu, C. H.; Kwong, D. L.; Chen, J. S. *Appl. Phys. Lett.* **2005**, *87*, 122101–122103.
(15) Lai, Y. S.; Tu, C. H.; Kwong, D. L.; Chen, J. S. *IEEE Electron Device Lett.* **2006**, *27*, 451–453.
(16) Teo, E. Y. H.; Ling, Q. D.; Tan, Y. P.; Wang, W.; Kang, E. T.; Chan, D. S. H.; Zhu, C. *Org. Electron.* **2006**, *7*, 173–180.
(17) Lin, J.; Ma, D. *Appl. Phys. Lett.* **2008**, *93*, 093505–093507.
(18) Ling, Q. D.; Song, Y.; Zhu, C. X.; Chan, D. S. H.; Kang, E. T.; Neoh, K. G. *Langmuir* **2007**, *23*, 312–319.
(19) Huang, C. M.; Liu, Y. S.; Chen, C. C.; Wei, K. H.; Sheu, J. T. *Appl. Phys. Lett.* **2008**, *93*, 203303–203305.
(20) Ouyang, J.; Chu, C. W.; Szmanda, C. R.; Ma, L.; Yang, Y. *Nat. Mater.* **2004**, *3*, 918–922.
(21) Yang, Y.; Ouyang, J.; Ma, L.; Tseng, R. J. H.; Chu, C. W. *Adv. Funct. Mater.* **2006**, *16*, 1001–1014.
(22) Tseng, R. J. H.; Baker, C. O.; Shedd, B.; Huang, J.; Kaner, R. B.;

Quyang, J.; Yang, Y. *Appl. Phys. Lett.* **2007**, *90*, 053101–053103.
(23) Lin, H. T.; Pei, Z.; Chen, Y. J. *IEEE Electron Device Lett.* **2007**, *28*, 569–571.
(24) Majumdar, H. S.; Baral, J. K.; Osterbacka, R.; Ikkala, O.; Stubb, H. *Org. Electron.* **2005**, *6*, 188–192.
(25) Kanwal, A.; Chhowalla, M. *Appl. Phys. Lett.* **2006**, *89*, 203103–203105.
(26) Laiho, A.; Majumdar, H. S.; Baral, J. K.; Jansson, F.; Osterbacka, R.; Ikkala, O. *Appl. Phys. Lett.* **2008**, *93*, 203309–203311.
(27) Baral, J. K.; Majumdar, H. S.; Laiho, A.; Jiang, H.; Kauppinen, E. I.; Ras, R. H. A.; Ruokolainen, J.; Ikkala, O.; Osterbacka, R. *Nanotechnology* **2008**, *19*, 035203–035209.
(28) Sugiyama, K.; Hirao, A.; Hsu, J. C.; Tung, Y. C.; Chen, W. C. *Macromolecules* **2009**, *42*, 4053–4062.
(29) Chi, C.; Wegner, G. *Macromol. Rapid Commun.* **2005**, *26*, 1532–1537.
(30) Lampert, M. A.; Mark, P. *Current Injection in Solids*; Academic Press: New York, 1970; p 59.
(31) Arif, M.; Yun, M.; Gangopadhyay, S.; Ghosh, K.; Fadiga, L.; Galbrecht, F.; Scherf, U.; Guha, S. *Phy. Rev. B* **2007**, *75*, 195202–195206.
(32) Dearnaley, G.; Stoneham, A. M.; Morgan, D. V. *Rep. Prog. Phys.* **1970**, *33*, 1129–1191.
(33) Kiriy, N.; Jhne, E.; Adler, H. J.; Schneider, M.; Kiriy, A.; Gorodyska, G.; Minko, S.; Jehnichen, D.; Simon, P.; Fokin, A. A.; Stamm, M. *Nano Lett.* **2003**, *3*, 707–712.
(34) Moule, A. J.; Meerholz, K. *Adv. Mater.* **2008**, *20*, 240–245.
(35) Li, L.; Lu, G.; Yang, X. *J. Mater. Chem.* **2008**, *18*, 1984–1990.

AM900346J